

Muon $g-2$ storage ring beam and spin dynamics

Editors: J. D. Crnkovic,^{1,*} D. W. Hertzog,² W. M. Morse,¹ and D. Stratakis³

(Muon $g - 2$ Collaboration)

¹*Brookhaven National Laboratory, Upton, New York 11973-5000, USA*

²*Department of Physics, University of Washington,
Seattle, Washington 98195-1560, USA*

³*Fermi National Accelerator Laboratory, Batavia Illinois 60510-5011, USA*

(Dated: February 22, 2020)

Abstract

Jason

The Fermilab Muon $g-2$ Experiment is currently collecting and analyzing data, where it has the goals of measuring the muon anomaly with 140 parts-per-billion (ppb) precision and electric dipole moment with at least 100 times more sensitivity than the previous measurement. The Fermilab experiment uses the refurbished and upgraded BNL Muon $g-2$ storage ring system, where these high precision measurements require a detailed understanding of the muon storage ring beam and spin dynamics for determining systematic corrections and uncertainties. The scintillating-fiber beam monitor, straw tracker, and calorimeter systems provide information about the storage ring beam, and detailed measurements and models of the storage ring guide fields have also been produced. The following discussion provides an overview of the Muon $g-2$ storage ring beam and spin dynamics, along with the associated systematic effects.

CONTENTS

I. Introduction	3
II. Determining the momentum distribution	4
III. Pitch	5
A. Pitch Correction	5
IV. Electric Field	6
A. E-field Correction	6
V. Fast Rotation	8
A. Fourier method	8
1. Start time	10
B. 9 parameter fit	11
C. Momentum time correlation	13
VI. Betatron Oscillations and E-field Systematic	13

* jcrnkovic@bnl.gov

Electrostatic quadrupole nonlinearity	13
Path length	15
E-field correction	15
Quadrupole Nonlinearity	16
Efield and pitch and Quadrupole Nonlinearity	17
Electric field contribution	18
Pitch	18
A. Efield - Equivalence of spin tracking and integration of ϕ_a .	19
B. Pitch - Equivalence of spin tracking and integration of ϕ_a .	19
C. Misalignment and Voltage errors	19
Simulation of Efield and pitch contributions to ω_a	19
References	20

I. INTRODUCTION

Jason

Muon dipole moment measurements [1–4] provide an important test of the Standard Model (SM), where the Brookhaven National Laboratory (BNL) Muon $g-2$ Experiment is the last completed experiment in a series of muon anomaly (a_μ) and electric dipole moment (d_μ) measurements. The Fermi National Accelerator Laboratory (Fermilab) Muon $g-2$ Experiment [5] is currently collecting and analyzing data, where it has completed the first physics data taking run (Run-1) and is now in the second physics data taking run (Run-2).

The Fermilab experiment can calculate a_μ from [5]

$$a_\mu = \left(\frac{g_e m_\mu \omega_a}{2 m_e \langle \omega_p \rangle} \right) / \left(\frac{\mu_e}{\mu_p} \right), \quad (1)$$

where g_e is the electron g-factor, m_μ/m_e is the muon-electron mass ratio, ω_a is the anomalous precession frequency, and μ_e/μ_p is the electron-proton magnetic moment ratio. The $\langle \omega_p \rangle$ in Eq. (1) corresponds to the average magnetic field seen by the muons, where the field has been written in terms of the corresponding free proton Larmor frequency because pulsed nuclear magnetic resonance (NMR) is used to measure the field. Values for g_e , m_μ/m_e , and

μ_e/μ_p can be obtained from CODATA [6], where these quantities have relative uncertainties of 0.000 26, 22, and 3.0 ppb respectively. The Fermilab experiment will measure ω_a and $\langle\omega_p\rangle$ to calculate the corresponding a_μ .

The final BNL a_μ value [7] has a relative statistical and systematic precision of 460 and 280 parts-per-billion (ppb) respectively, for a total precision of 540 ppb when adding the two uncertainties in quadrature. There is a greater than 3σ difference between the BNL measurement and SM prediction [7], which hints at the possibility of physics beyond the SM. The Fermilab experiment has the goal of measuring a_μ with a final statistical and systematic precision of 100 ppb respectively, for a total precision of 140 ppb when adding the two uncertainties in quadrature. The 100 ppb statistical uncertainty is for ω_a , as the statistical uncertainty for $\langle\omega_p\rangle$ is negligible, and the ω_a and $\langle\omega_p\rangle$ measurements are to each have a 70 ppb systematic precision. The BNL $|d_\mu| < 1.8 \times 10^{-19} e \text{ cm}$ (95% C.L.) measurement provides a factor of 5 improvement in sensitivity with respect to the previous limit, and the Fermilab experiment has the goal improving the sensitivity by at least a 100 times with respect to the BNL measurement.

Achieving a 70 ppb systematic precision for ω_a requires a detailed understanding of the muon storage ring beam and spin dynamics. The Fermilab experiment uses the refurbished and upgraded BNL muon storage ring system, where the following discussion describes the storage ring magnetic and electric guide fields, lattice functions, tunes, closed orbits, polarized muon injection, and storage of the muons. The scintillating-fiber beam monitor (FBM), straw tracker, and calorimeter systems are also discussed, as these systems provide information about the storage ring beam. Finally, an overview of the known ω_a systematic effects that arise from beam and spin dynamics is also given.

DAVE RUBIN HAS Fast Rotation, Electric Field, and Pitch section as of 1/21/20

II. DETERMINING THE MOMENTUM DISTRIBUTION

???

III. PITCH

A. Pitch Correction

David R.

The projection of polarization onto velocity is given by (Jackson 11.171)

$$\frac{d}{dt}(\hat{\beta} \cdot \mathbf{s}) = -\frac{e}{mc} \mathbf{s}_\perp \cdot \left[a_\mu (\hat{\beta} \times \mathbf{B}) + \left(a_\mu - \frac{1}{\gamma^2 - 1} \right) \beta \mathbf{E} \right]. \quad (2)$$

For the component of the spin that is precessing in the ρ, ϕ plane $\mathbf{s} = s(\hat{\phi} \cos \omega_a t + \hat{\rho} \sin \omega_a t)$.

Then for the ideal trajectory, Equation 2 becomes

$$\frac{d}{dt} s \cos \omega_a t = -\frac{e}{mc} s \sin \omega_a t (a_\mu B)$$

and

$$\omega_a = -\frac{e}{mc} a_\mu B.$$

The dependence of ω_a on the amplitude of vertical betatron oscillations appears in the term $\hat{\beta} \times \mathbf{B}$ in Eq. (2). Introduce the vertical component of velocity as a small perturbation, so that $\hat{\beta} = \cos \psi_{y\phi} \hat{\rho} + \sin \psi_{y\phi} \hat{y}$, where $\psi_{y\phi}$ is the angle of the trajectory of the muon in the $y - \phi$ plane. $\hat{\phi}$ is the unit vector in the azimuthal direction. Then the contribution to ω_a due to the pitch for a particular trajectory is $\frac{\Delta\omega_a}{\omega_a} = \langle (1 - \cos \psi_{y\phi}) \rangle$, where the $\langle \rangle$ indicate the average of $(1 - \cos \psi_{y\phi})$ along the trajectory. For small pitch angle, $\psi_{y\phi} \ll 1$,

$$\frac{\Delta\omega_a}{\omega_a} \sim \frac{1}{2} \langle \psi_{y\phi}^2 \rangle.$$

In the limit of strictly linear betatron motion, the angle of the trajectory in the $y - \phi$ plane is modulated as

$$\psi_{y\phi}(s) = \psi_0 \sin \phi_y(s) = \sqrt{\frac{a}{\beta_y}} \sin \phi_y(s),$$

where $\phi_y(s)$ is the vertical betatron phase advance as a function of longitudinal position s and

$$\langle \psi_{y\phi}^2 \rangle = \frac{1}{2} \psi_0^2 = \frac{1}{2} \frac{a}{\beta}$$

and the average is taken over many betatron periods. We do not measure the distribution of amplitudes directly but rather the distribution of vertical offsets. Insofar as

$y = \sqrt{a\beta} \cos \phi(s)$, then $\langle y^2 \rangle = \frac{1}{2}\beta\langle a \rangle$ and $\langle a \rangle = 2\langle y^2 \rangle/\beta$. Then averaged over betatron phase and amplitude

$$\langle \psi_{y\phi}^2 \rangle = \frac{\langle y^2 \rangle}{\beta^2}$$

Finally the average correction to ω_a due to the vertical betatron motion is

$$\left\langle \frac{\Delta\omega_a}{\omega_a} \right\rangle_a \sim \frac{1}{2} \frac{\langle y^2 \rangle}{\langle \beta \rangle^2}.$$

$\langle \beta \rangle = (\int_{\text{accept}} \beta(s) ds) / s_{\text{accept}}$ is the average over the azimuthal acceptance of the tracking chambers that measure the vertical distribution. In the continuous quad limit, where $1/\beta_y = \frac{\sqrt{n}}{R_0}$.

$$C_p = -\frac{n\langle y^2 \rangle}{2R_0^2}$$

The vertical distribution of decay positrons is measured by the straw tracking chambers. Tracks of positrons are extrapolated back to the parent muon decay point to determine the vertical distribution of the muons as shown for a subset of the data in Fig. 1.

IV. ELECTRIC FIELD

A. E-field Correction

David R.

In the rest frame of the muon the transverse electric field manifests as a magnetic field and alters the instantaneous precession frequency, as defined by the third term on the right hand side of Eq. (2). It depends on muon momentum and the effect is minimized by operating near the magic momentum, namely where $a_\mu = \frac{1}{\gamma^2 - 1} = a_\mu - \frac{m^2}{p_m^2}$. The field of the ring magnet is chosen so that the closed orbit of the magic momentum muon corresponds to the center of the good field region. Then the fractional contribution to ω_a is

$$C_e \sim -2 \frac{\Delta p}{p_m} \frac{|\langle \vec{\beta} \times \vec{E} \rangle|}{Bc}, \quad (3)$$

where p_m is the magic momentum, and γ and β are evaluated at p_m and averaged along the trajectory of the muon. The electric field depends on transverse displacement in the quadrupoles. Insofar as the field is linear in displacement, the average electric field along

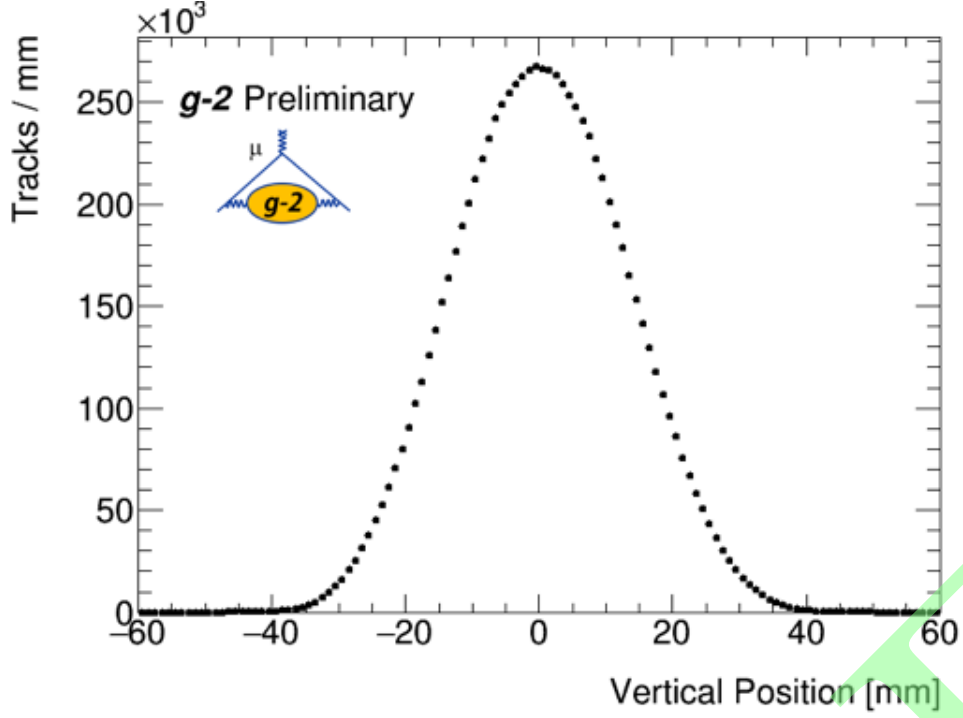


FIG. 1. Vertical projection of decay muons from straw trackers

the trajectory is proportional to the average radial displacement x_e , namely the closed orbit. The average radial electric field is given by

$$\langle E_r \rangle = n \left(\frac{v_s B}{R_0} \right) x_e, \quad (4)$$

where n is the focusing index. The average radial displacement is

$$x_e = \eta \frac{\Delta p}{p}.$$

Then the contribution to ω_a due to electric field is

$$C_e \sim -2\beta^2 n(1-n) \frac{x_e^2}{R_0^2},$$

where $\eta \approx \frac{1-n}{R_0}$. Determination of the electric-field correction thus depends on measurement of the equilibrium radial distribution.

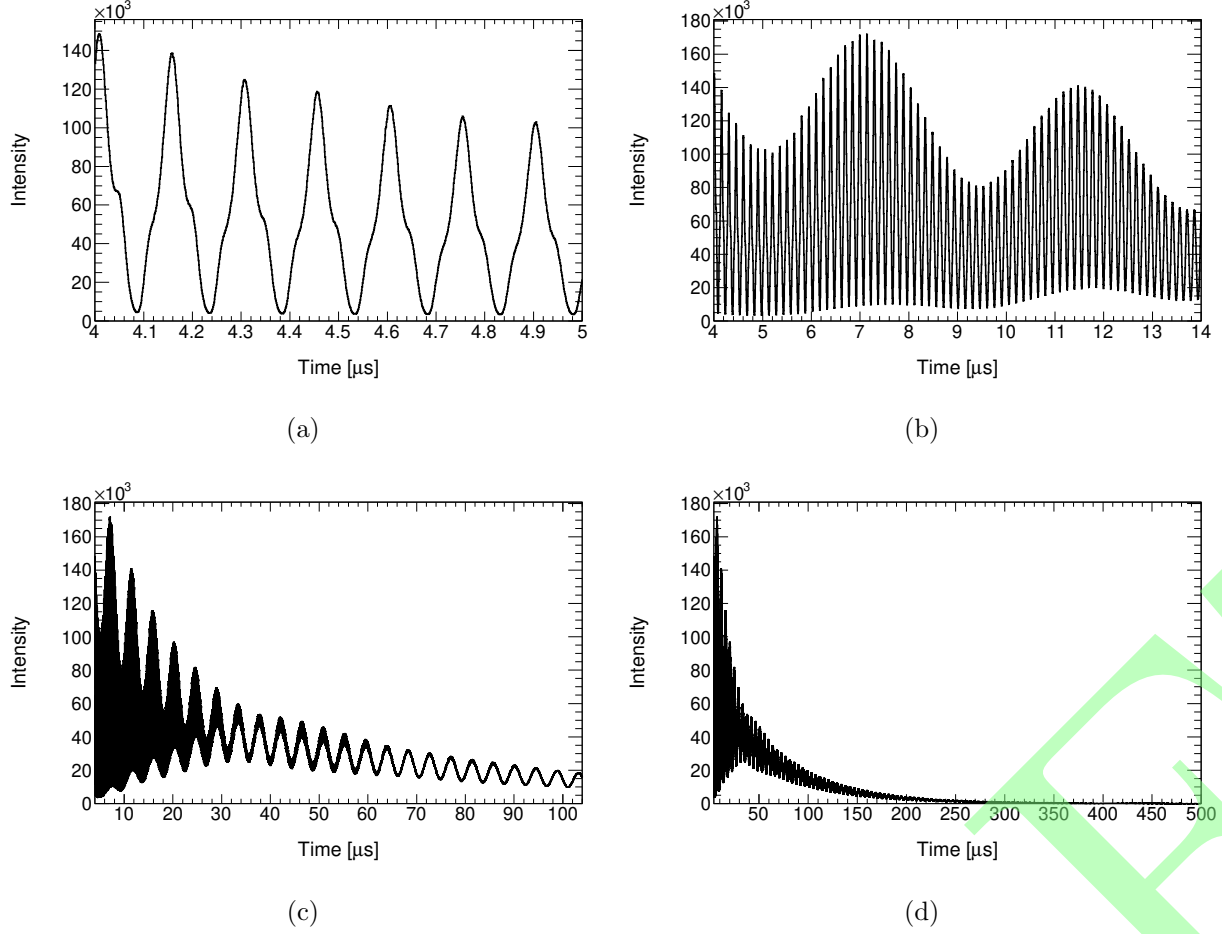


FIG. 2. Positron counts as a function of time as seen by all the calorimeters combined for the Run-1 9-day data set for the time ranges: (a) 4-5, (b) 4-14, (d) 4-104 and (e) 4-500 μs with respect to the beam injection. The time interval is 1 ns.

V. FAST ROTATION

The contribution to the measured precession frequency of the electric field depends on the momentum distribution of the stored muon beam, or equivalently the equilibrium radial distribution. The muon revolution frequency is inversely proportional to its momentum. A technique [8] based on Fourier transform yields a frequency spectrum that can be correlated with radius (circumference) and momentum. The fast rotation data is provided by the calorimeters which measure the time dependence of the intensity of the decay positron distribution. The positron counts from the 24 calorimeters are merged together with time offset of $T/24/\text{calorimeter}$ where T is the revolution period of the magic momentum muon.

A. Fourier method

The intensity profile of a distribution with zero emittance, zero momentum spread and zero bunch length, measured at a fixed point in the ring, is

$$I(t) = \sum_{n=0}^{\infty} \delta(t - t_0 - nT) \quad (5)$$

where n includes all nonnegative integers. (For the moment we ignore the finite lifetime of the muon.) If we extend Equation 5 to include all integers then $I(t)$ is symmetric about $t = t_0$ and the Fourier transform is simply a cosine transform. The frequency spectrum is the cyclotron frequency $\omega_c = 2\pi/T$ and all of its harmonics.

$$F(\omega) = \sum_{n=-\infty}^{\infty} \cos n\omega T \quad (6)$$

The cosine transform of the signal for $n \geq 0$, is equivalent to the Fourier transform of the signal that includes a symmetric extension to negative times. The revolution period is $T(1 + \Delta)$ for particles with fractional momentum offset Δ and

$$I(t, \Delta) = \sum_n \delta(t - t_0 - nT(1 + \Delta))$$

and if $\rho(\Delta)$ is the distribution of momentum offsets,

$$S(t) = \sum_n \int (\rho(\delta) \delta(t - t_0 - nT(1 + \Delta)) d\Delta$$

The fast rotation signal is linear in particle momentum, and the cosine transform linear in frequency so that

$$\hat{S}(\omega) = \int S(t) \cos \omega t = \int \cos \omega t \sum_n \int (\rho(\delta) \delta(t - t_0 - nT(1 + \Delta)) d\Delta dt$$

The distribution of muons injected into the ring extends over some finite time duration. Suppose that some fraction of the distribution corresponds to

$$S(t)_{early} = \sum \delta(t - t_0 - \Delta t - nT).$$

$S(t)_{early}$ is not symmetric about $t = t_0$ and the fourier transform of the signal symmetrized about $t = t_0$ will include a sine as well as a cosine term. However, if the injected distribution is symmetric about $t = t_0$ such that $S(t - t_0 - \Delta t)_{late} = S(t - t_0 + \Delta t)_{early}$, that is

$$S(t) = \sum \delta(t - t_0 - \Delta t - nT) + \sum \delta(t - nT) + \sum \delta(t - t_0 + \Delta t - nT),$$

then the sine term vanishes once again. In practice we define t_0 to be the time that best symmetrizes the frequency distribution.

1. Start time

The fast rotation signal is contaminated during the first few microseconds (a few tens of revolutions) of the fill by background from positrons, protons, and deuterons. As a result

$$S(t) = \sum_{n=n_{start}} \int \rho(\Delta) \delta(t - t_0 - nT(1 + \Delta)) d\Delta$$

where $n_{start} \sim 25$, and unphysical frequencies appear in the cosine transform. The particles were there, we just could not see them. We refer to the distortion of the spectrum that arises from the gap in our measurement of the fast rotation signal as 'background'. We write

$$\hat{S}(\omega) = \sqrt{\frac{2}{\pi}} \int_{t_s}^{\infty} S(t) \cos \omega t dt + \sqrt{\frac{2}{\pi}} \int_{t_0}^{t_s} S(t) \cos \omega t dt$$

where $S(t)$ is measured over the interval $t_s \rightarrow t_{\infty}$. Define

$$\begin{aligned} \hat{S}'(\omega) &= \sqrt{\frac{2}{\pi}} \int_{t_s}^{\infty} S(t) \cos \omega t dt \\ \Delta(\omega) &= \sqrt{\frac{2}{\pi}} \int_{t_0}^{t_s} S(t) \cos \omega t dt \end{aligned}$$

To a first approximation

$$S_0(t) = \int_{\omega_-}^{\omega_+} \hat{S}'(\omega') \cos \omega' t d\omega'$$

where the limits of integration correspond to the range of momenta within the physical aperture of the ring. Then

$$\begin{aligned} \Delta(\omega) &= \sqrt{\frac{2}{\pi}} \int_{t_0}^{t_s} S_0(t) \cos \omega t dt \\ &= \frac{2}{\pi} \int_{t_0}^{t_s} \int_{\omega_-}^{\omega_+} \hat{S}'(\omega') \cos \omega' t \cos \omega t d\omega' dt \\ &= \frac{1}{\pi} \int_{\omega_-}^{\omega_+} \hat{S}'(\omega') \left(\frac{\sin(\omega' + \omega)(t_s - t_0)}{\omega' + \omega} + \frac{\sin(\omega' - \omega)(t_s - t_0)}{\omega' - \omega} \right) d\omega' \\ &\sim \frac{1}{\pi} \int_{\omega_-}^{\omega_+} \hat{S}'(\omega') \frac{\sin(\omega' - \omega)(t_s - t_0)}{\omega' - \omega} d\omega' \end{aligned}$$

In practice we guess an appropriate functional form for $\hat{S}'(\omega)$ and fit the parameters of the function to the background. If the spectrum is a Dirac comb at the revolution frequency then from Equation 6 we see that a first approximation might be

$$\hat{S}'(\omega) \sim \sum_{n=0}^{n_{start}} \cos n\omega T = \sum_{n=0}^{n_{start}} \cos n(\omega_c + \delta\omega)T = \sum_{n=0}^{n_{start}} \cos(n\delta\omega T)$$

As long as $n_{start}\delta\omega T \ll 1 \rightarrow n_{start}$, then we can expand the cosine in an even power series, and indeed in that limit, a polynomial fits the background. The spread in frequencies is limited by the momentum acceptance of the storage ring to $\delta\omega/\omega_0 < \pm 0.6\% \rightarrow n_{start} \ll 25$ turns or $\sim 4\mu s$. More sophisticated functional forms have been demonstrated to give good background fits for start times up to $t_{start} \sim 25\mu s$ in Monte Carlo simulation. Further the fitted spectrum is very nearly independent of start time for $4\mu s < t_{start} < 25\mu s$.

B. 9 parameter fit

In addition to revolution frequencies the time dependence of the intensity of the positrons will include the horizontal betatron oscillation frequency, the muon precession frequency, and the muon decay time. In order to mitigate contamination of the Fourier analysis of revolution frequencies, we divide the fast rotation data by a nine parameter fitted function

$$N(t) = N_0 e^{-t/\tau_\mu} [1 + A \cdot \cos(\omega_a t + \phi)] \cdot e^{-t/\tau_{cbo}} [1 + A_{cbo} \cdot \cos(\omega_{cbo} t + \phi_{cbo})]. \quad (7)$$

where N_0 is the number of detected positrons at $t = 0$, τ_μ is the muon boosted life-time of about $64\mu s$, A is the asymmetry of the spin precession modulation, ω_a the anomalous spin precession frequency and ϕ the phase of the modulation, A_{cbo} , ω_{cbo} and τ_{cbo} , and ϕ_{cbo} the amplitude, frequency, 'lifetime' and phase of the coherent betatron oscillation

An example of radial (closed orbit) distribution extracted by both the Fourier method and the debunching analysis are shown in Fig. ???. The dependence of the E-field contribution to ω_a , on the radial offset of the closed orbit, superimposed on the the measured distribution is shown in Fig. ???.

C. Momentum time correlation

VI. BETATRON OSCILLATIONS AND E-FIELD SYSTEMATIC

The contribution of the electric field correction to the measured ω_a in IV A assumes that the magnitude of the radial electric field increases linearly with displacement from the magic radius, and that the betatron tune is independent of amplitude and momentum. Because the plates that support the quadrupole voltage are flat, the electric field necessarily rolls off near the plates. Effective vertical focusing, decreases with displacement from the central

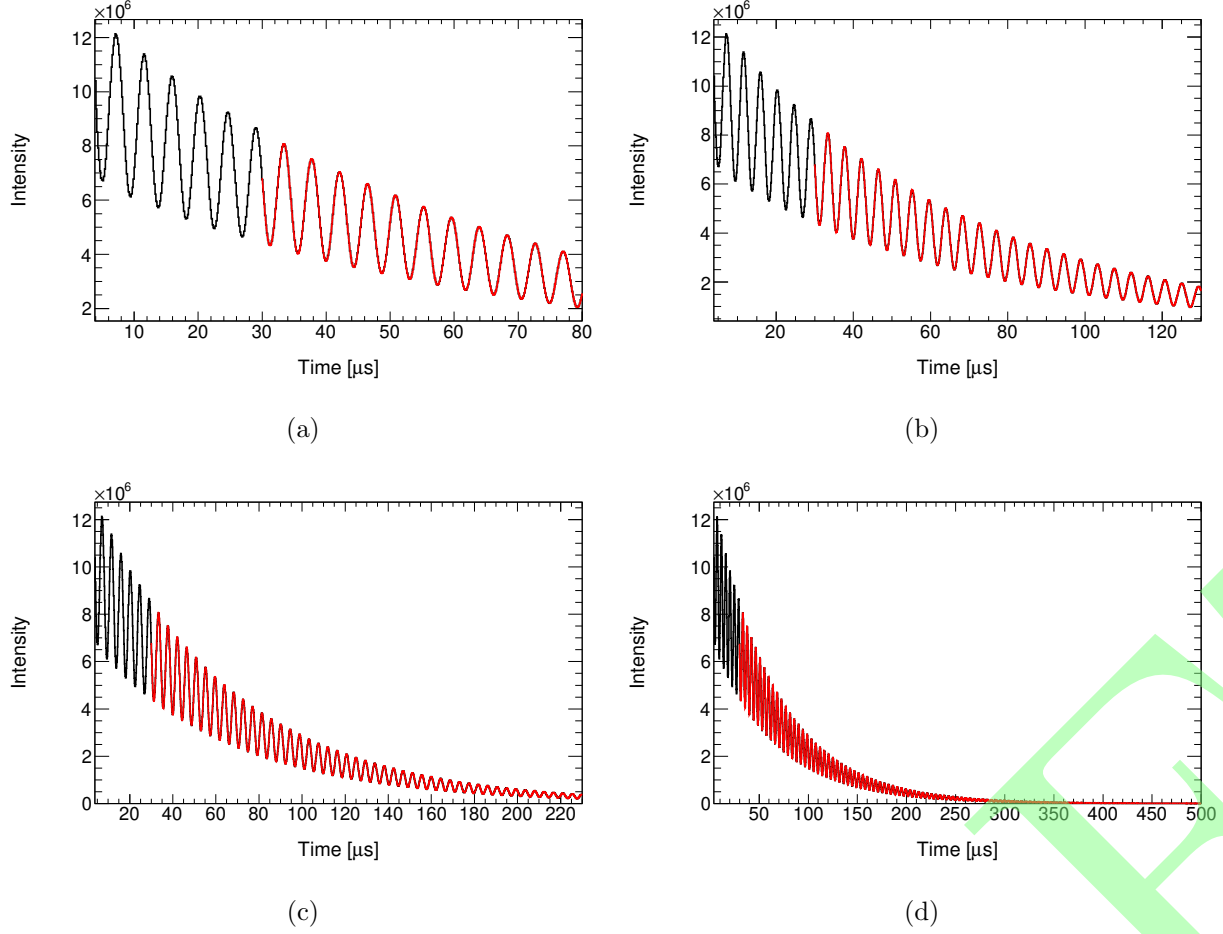


FIG. 3. Fit of the positron counts histogram as a function of time as seen by all the calorimeters combined for the Run-1 9-day data set for the time ranges: (a) 4-80, (b) 4-130, (d) 4-230 and (e) 4-500 μs with respect to the beam injection. The time interval is 149 ns.

orbit. The vertical tune will decrease and the horizontal increase for large amplitudes and for particles near the momentum aperture. As long as the electric field is antisymmetric about the design orbit, the average electric field along the trajectory of the muon will be independent of the amplitude of any betatron oscillation. However, because of the finite curvature of the quadrupoles, the E-field correction to ω_a there is necessarily a quadratic dependence of electric field on displacement. The muon that circulates at the magic radius with zero betatron oscillation amplitude will see zero electric field and no correction is required. But the muon with that same momentum and finite betatron amplitude will oscillate about the magic radius and its precession will indeed be effected by the E-field. If the quad field were strictly antisymmetric about the magic radius and the betatron trajectory

strictly symmetric, the net contribution would be zero. But neither condition is true. We consider first the origin and effect of a sextupole like component of the 'perfect' quadrupole analytically and then evaluate the effect of nonlinearity associated with the geometry of the quadrupoles, including misalignment of the plates and voltage errors.

Electrostatic quadrupole nonlinearity

Consider the electric field in the quadrupoles. Laplace's equation in two dimensions and cartesian coordinates is

$$\nabla^2 V(x, y) = \frac{\partial^2 V}{\partial x^2} + \frac{\partial^2 V}{\partial y^2} = 0 \quad (8)$$

The potential corresponding to a pure quadrupole field is one (of many) solutions.

$$V = \frac{1}{2}k(x^2 - y^2)$$

for some constant k . The electric field is

$$E = \vec{\nabla}V = k(x\hat{i} - y\hat{j})$$

and of course the divergence is zero. The electric field is linear in both x and y . Higher order terms may appear (and indeed in the g-2 quads they will appear due to the geometry of the plates), but the symmetry (in the 2-D cartesian limit permits only those terms that are odd in x, y . In particular there is no sextupole ($\sim kx^2$) dependence that would be symmetric in displacement.

In the limit of finite curvature (as in the g-2 geometry) it is more appropriate to represent the fields in cylindrical coordinates, where Laplace's equation is

$$\nabla^2 V(\rho, z, \phi) = \left(\frac{1}{\rho} \frac{\partial}{\partial \rho} \left(\rho \frac{\partial}{\partial \rho} \right) + \frac{1}{\rho^2} \frac{\partial^2}{\partial \theta^2} + \frac{\partial^2}{\partial z^2} \right) V = 0$$

We assume the quads are continuous so that there is no dependence on the angular coordinate ϕ . Then the simplest possible solution is

$$V(\rho, z) = k \left(\frac{1}{2} \left(\frac{\rho^2}{\rho_0^2} - 1 \right) - \ln \frac{\rho}{\rho_0} - \left(\frac{z}{\rho_0} \right)^2 \right)$$

and the electric field

$$\vec{\nabla}V = \frac{1}{2}k \left(\left(\rho - \frac{\rho_0^2}{\rho} \right) \hat{\rho} - 2z\hat{z} \right) \quad (9)$$

If we write $\rho = \rho_0 + x$ where ρ_0 is the magic radius, then

$$\vec{E} \sim k \left(\left(x - \frac{x^2}{2\rho_0} + \dots \right) \hat{\rho} - z \hat{z} \right) \quad (10)$$

Evidently, Maxwell's equations require a term quadratic in displacement. The quadratic term is equivalent to a sextupole-like component that will effect the chromaticity, complicate the correction of the E-field systematic, and possibly drive a third order resonance.

The above solution is not unique. One can write alternative solutions where the quadratic (x^2) term does not appear in the radial field, but then it always turns up as (xz) in the vertical direction. There exist no solutions without some sextupole-like component. A fit to a 3 dimensional field map would properly identify this term.

There exists a symmetric component of the E-field which will contribute to the E-field systematic.

Path length

The radial electric field along the trajectory of a muon with equilibrium radial offset x_e and betatron amplitude x_β is

$$E_r(s) = k(x_e + x_\beta) - \frac{1}{2\rho_0}(x_e + x_\beta)^2 + \dots$$

$$E_r(s) = k(\eta\delta + x_\beta) - \frac{1}{2\rho_0}(\eta\delta + x_\beta)^2 + \dots$$

where $x_e = \eta\delta = \eta \frac{\Delta p}{p}$ and we assume the 'simple' solution to Laplace's equation discussed above. The muon trajectory is along the path dl as shown in Figure 8. The path s is the reference orbit. The average electric field along the trajectory is

$$\langle E_r(s) \rangle = k \left\langle \left(\eta\delta + x_\beta - \frac{1}{2\rho_0}(\eta\delta + x_\beta)^2 \right) \right\rangle \quad (11)$$

$$= \frac{k}{L} \int_0^L \left(\eta\delta + x_\beta - \frac{1}{2\rho_0}(\eta\delta + x_\beta)^2 \right) dl \quad (12)$$

$$= \frac{k}{L} \int_0^L \left(\eta\delta + x_\beta - \frac{1}{2\rho_0}(\eta\delta + x_\beta)^2 \right) (1 + x_\beta/\rho_0) ds \quad (13)$$

here in that last step we use $d\phi = \frac{ds}{\rho_0} = \frac{dl}{(\rho_0+x)}$, and L is the length of the trajectory. Using $x_\beta = x_{\beta 0} \cos \phi(s)$, $\langle E_r \rangle$ becomes

$$\begin{aligned} \langle E_r(s) \rangle &= k \int \left(\eta\delta + x_{\beta 0} \cos \phi - \frac{1}{2\rho_0} (\eta\delta + x_{\beta 0} \cos \phi)^2 \right) d\phi (1 + x/\rho_0) \\ &\sim k \left(\eta\delta + \frac{1}{2\rho_0} ((\eta\delta)^2 + \frac{1}{2} x_{\beta 0}^2) + \dots \right) \end{aligned} \quad (14)$$

There is contribution to the average electric field that scales quadratically with the betatron amplitude.

E-field correction

Substitution of Equation 14 into 4 gives the correction to ω_a due to fractional momentum offset δ and betatron amplitude $x_{\beta 0}$ as

$$\begin{aligned} C_e(\delta, x_{\beta 0}) &\approx -2\delta \frac{\beta k}{cB} \left(\eta\delta + \frac{1}{2\rho_0} ((\eta\delta)^2 + \frac{1}{2} x_{\beta 0}^2) \right) \\ &\approx 2 \frac{\beta k}{cB} \left(\eta\delta^2 + \frac{1}{2\rho_0} (\eta^2\delta^3 + \frac{1}{2} x_{\beta 0}^2 \delta) \right) \end{aligned}$$

Next we need to average $C_e(\delta, x_{\beta 0})$ over the entire momentum and CBO distribution.

$$\langle C_e(\delta, x_{\beta 0}) \rangle \approx -2 \frac{\beta k}{cB} \left(\frac{\langle x_e^2 \rangle}{\eta} + \frac{1}{2\rho_0} \left(\frac{\langle x_e^3 \rangle}{\eta} + \frac{1}{2} \langle x_{\beta 0}^2 \rangle \frac{\langle x_e \rangle}{\eta} \right) \right)$$

where $\langle \delta \rangle = \langle x_e \rangle / \eta$. If $\langle \delta \rangle = \langle x_e \rangle / \eta = 0$, and we assume that the betatron amplitude and momentum offset are uncorrelated. In fact momentum offset and betatron amplitude are strongly anti-correlated. We will return to this point.

$$\langle C_e(\delta, x_{\beta 0}) \rangle = -2 \frac{\beta k}{cB} \eta \langle \delta^2 \rangle$$

and there is no contribution from the sextupole or path length terms. If $\langle \delta \rangle \neq 0$ then the fractional change to the E-field correction is

$$\frac{\Delta C_e}{C_e} \sim \frac{\langle x_e^3 \rangle + \langle x_e \rangle \langle x_{\beta 0}^2 \rangle / 2}{2 \langle x_e^2 \rangle \rho_0}$$

If we very conservatively estimate that $\langle x_{\beta 0}^2 \rangle < 45^2 \text{mm}^2$, then

$$\frac{\Delta C_e}{C_e} < 4.9^{-3}$$

We find that the change in the efield correction due to the nonlinearity associated with the curvature of the quad plates, is less than 0.5%.

Quadrupole Nonlinearity

In the previous section we studied the effect of the curvature of the quadrupoles that is the origin of a sextupole like (symmetric) electric field. The rectangular cross section of the quadrupole geometry introduces nonlinearity. The electric field along the horizontal axis ($y = 0$) is given by

$$E_x - iE_y = (b_n - ia_n) \frac{x^n}{r_0^n} \quad (15)$$

where $r_0 = 0.045$ m and a_n, b_n are given in Table ???. The multipoles are computed as a fit to an azimuthal slice of the 3D Opera field map of the quads[?]. The fit is for a 'horizontally' pure basis[?][?] of Mcmillan functions. Figure VI shows the horizontal electric field in the midplane. The values from the Opera map, and from the multipole expansion are superimposed and evidently are in excellent agreement.

We can compare the fitted sextupole-like coefficient to our 'guess' discussed above. We found a solution to the Laplacian in the curved system as Equation 10. The ratio of the coefficients of the quadratic and linear terms is $r_{hyp} - \frac{1}{2\rho_0} = -0.0703\text{m}^{-1}$. But that 'hypothetical' solution is not unique. After all, while we insisted on a form that satisfies Maxwell's equations, we made no attempt to also satisfy the boundary conditions. The ratio based on the fit to the Opera field map, that satisfies both Maxwell and the boundary conditions, taking the values from the table is $r_{fit} = \frac{b_2}{b_1 r_0} = -2.71281 \times 10^3 / 1.01609 \times 10^6 = -0.0593\text{m}^{-1}$, within 16% of our guess.

As was shown above, the effect of the sextupole-like component of the quadrupole, and the asymmetry of the path length about the magic radius, is that the E-field correction depends on betatron amplitude and nonlinearly on equilibrium radial offset. From Equations 11- 13 we see that the sextupole-like component and the path length contribute with opposite sign, and the amplitude of the sextupole-like component is about 1/2 of the path length piece. Based on measured equilibrium radial distribution we conclude that the contribution of the sextupole-like component to the E-field correction is less than 1%.

There are in addition to the sextupole-like component higher order multipoles as evident from the table. In particular we see in Fig. VI that the field gradient rolls off at large amplitudes.

Since the quad plate is an equipotential surface, the component of the electric field parallel to the plate vanishes near the surface. Then $\vec{\nabla} \cdot \vec{E} = 0 \rightarrow \frac{\partial E_{\perp}}{\partial dx_{\perp}} \rightarrow 0$. Near the plates, the

quad index $n \rightarrow 0$. We explore the implications in simulation.

EFIELD AND PITCH AND QUADRUPOLE NONLINEARITY

In simulation ω_a is most directly determined by spin tracking. The trajectory of the muon is established by numerically integrating the equations of motion, and the spin by integration of the BMT equation along that trajectory. We would like to explore the contribution to ω_a numerically, due the electric field of the quads and the vertical pitching (vertical betatron motion), so that we can incorporate nonlinearity that arises from the quadrupole geometry, and alignment errors. Spin tracking includes both effects. But spin tracking is inconvenient for at least 3 reasons

1. Integration of the BMT equation is computationally intensive (and slow).
2. The change in ω_a due to the electric field and the pitch is of order 1 part in 10^7 . Extracting their contribution depends on the difference of large numbers, and subject to error.
3. There is no simple way to distinguish contributions from electric field, and pitch, and whatever else.

As an alternative to spin tracking, we revisit the expressions for the contributions to Efield and pitch and proceed as follows.

Electric field contribution

Recall that electric field appears as

$$\vec{\omega}_a = -\frac{q}{m} \left[a_\mu \vec{B} \left(a_\mu - \frac{m^2}{p^2} \right) \frac{\vec{\beta} \times \vec{E}}{c} \right] \quad (16)$$

Define $\phi_a = \int_0^T \omega_a dt$. In the absence of \vec{E} , we compute ϕ_a by integrating \vec{B}_\perp along the muon trajectory. Evidently, the contribution from the the electric field to ϕ_a is given by

$$\frac{\Delta\phi_E}{\phi_a} = \left(a_\mu - \frac{m^2}{p^2} \right) \frac{1}{c} \int_0^T \vec{\beta} \times \vec{E} dt \approx -2 \frac{\Delta p}{p} \frac{1}{c} \int_0^T \vec{\beta} \times \vec{E} dt \quad (17)$$

where $\Delta p = p - p_{magic}$. In the tracking code it is straightforward to compute the sums in Equations 16 and 17. Then the electric field correction for the trajectory is

$$C_e(T) = -2 \frac{\Delta p}{p} \frac{1}{T} \int^T \frac{\vec{\beta} \times \vec{E}}{Bc} dt \quad (18)$$

(We assume that \vec{B} is parallel to $\vec{\beta} \times \vec{E}$.)

Pitch

Consider the trajectory shown in 10 of a muon executing betatron oscillations in the vertical plane. The pitching angle is ψ_0 . The magnetic field is in the vertical direction and y_0 is the associated vertical displacement. We are interested in the precession of the spin with respect to the muon momentum and therefore its projection onto the plane that contains the velocity and $\vec{\beta} \times \vec{B}$. The component of the magnetic field along the perpendicular to the plane is $B_{\perp} = B \cos \psi$. The spin tune, that is the advance of the spin phase per turn is then

$$\nu_{spin} = \oint B_{\perp} dl = \oint B \cos \psi dl \quad (19)$$

where the integration is through a single turn. The path length of the pitching trajectory is

$$\oint \sqrt{dx^2 + dy^2} = \oint \sqrt{1 + \left(\frac{dy}{dx}\right)^2} dx \sim \oint 1 + \frac{1}{2} \psi_0^2 \sin^2\left(\frac{2\pi y}{L}\right) = L \left(1 + \frac{1}{4} \psi_0^2\right) \quad (20)$$

The pathlength increases with the square of the pitching angle. Therefore the spin tune is independent of the pitching angle. On the other hand, the cyclotron frequency decreases with pitching angle according to $\omega_c(\psi_0) \sim \omega_c(0) \left(1 - \frac{1}{4} \psi_0^2\right)$ and then

$$\omega_a(\psi_0) = \omega_a(0) \left(1 - \frac{1}{4} \psi_0^2\right)$$

Then

$$\frac{\Delta \phi_p}{\phi_a} = \frac{1}{T} \int^T (|B| - |\hat{\beta} \times B|) dt \quad (21)$$

- A. Efield - Equivalence of spin tracking and integration of ϕ_a .
- B. Pitch - Equivalence of spin tracking and integration of ϕ_a .
- C. Misalignment and Voltage errors

SIMULATION OF EFIELD AND PITCH CONTRIBUTIONS TO ω_a

In simulation, the electric field of each of the quad plates (inner, bottom, outer, top) is based on a field map. The map for each plate is computed with OPERA, holding the other three plates at zero potential. The field of the quadrupole is then a simple superposition of the four maps. The maps that are implemented in the code are 2D azimuthal slices of the full 3D map. Curvature of the plates is modeled correctly. End fringe fields are neglected.

As indicated in Fig. 18, the quad plates can be displaced and/or voltage errors introduced on each plate. We explore the dependence of the contribution of the electric field, and pitch to ω_a on these alignment and field errors.

1. Implement the quad plate offsets and voltage errors in the BMAD model
2. Create a 'realistic' distribution
3. Track the distribution through the injection channel and into the ring.
4. Track each muon until it decays.
5. For each muon
 - Integrate $\vec{\beta} \times \vec{E}$ along the trajectory to determine the electric field contribution to ω_a
 - Integrate $(1 - |\beta \times \vec{B}|)$ along the trajectory to determine the contribution from pitch
 - Compute radial closed orbit $\langle x_e \rangle$
6. Use the 'measured' radial and vertical coordinates (positions and times) at the decay point to compute the betatron tunes for the distribution.

7. Use the 'measured' vertical coordinate (positions) at the decay point to determine vertical distribution

The alignment of the plates is measured with an uncertainty of less than $\pm 1\text{mm}$. The uncertainty in voltage is estimated to be within $\pm 5\%$. A particular set of alignment and field errors defines a configuration. For each of the four plates there are two possible displacement errors ($\pm 1\text{mm}$), and two possible voltage errors $\pm 0.05V$, for a total of $N_Q = 2^8 = 256$ configurations for a single quad. Each configuration corresponds to a maximum set of misalignments and field errors. There are eight quadrupoles and therefore $N_T = (2^8)^8$ configurations for all quads. There is significant repetition due to the geometric periodicity, but even so there are far too many independent configurations to consider.

-
- [1] G. Charpak *et al.*, A New Measurement of the Anomalous Magnetic Moment of the Muon, *Phys. Lett.* **1**, 16 (1962).
 - [2] J. Bailey *et al.* (CERN-Mainz-Daresbury), Final Report on the CERN Muon Storage Ring Including the Anomalous Magnetic Moment and the Electric Dipole Moment of the Muon, and a Direct Test of Relativistic Time Dilation, *Nucl. Phys.* **B150**, 1 (1979).
 - [3] G. W. Bennett *et al.* (Muon g-2), Final Report of the Muon E821 Anomalous Magnetic Moment Measurement at BNL, *Phys. Rev.* **D73**, 072003 (2006), [arXiv:hep-ex/0602035](https://arxiv.org/abs/hep-ex/0602035) [hep-ex].
 - [4] G. W. Bennett *et al.* (Muon (g-2)), An Improved Limit on the Muon Electric Dipole Moment, *Phys. Rev.* **D80**, 052008 (2009), [arXiv:0811.1207](https://arxiv.org/abs/0811.1207) [hep-ex].
 - [5] J. Grange *et al.* (Muon g-2), Muon (g-2) Technical Design Report, (2015), [arXiv:1501.06858](https://arxiv.org/abs/1501.06858) [physics.ins-det].
 - [6] P. J. Mohr *et al.*, CODATA Recommended Values of the Fundamental Physical Constants: 2014, *Rev. Mod. Phys.* **88**, 035009 (2016), [arXiv:1507.07956](https://arxiv.org/abs/1507.07956) [physics.atom-ph].
 - [7] M. Tanabashi *et al.* (Particle Data Group), Review of Particle Physics, *Phys. Rev.* **D98**, 030001 (2018).
 - [8] Y. Orlov *et al.*, Muon revolution frequency distribution from a partial-time Fourier transform of the g-2 signal in the muon g-2 experiment, *Nucl. Instrum. Meth.* **A482**, 767 (2002).

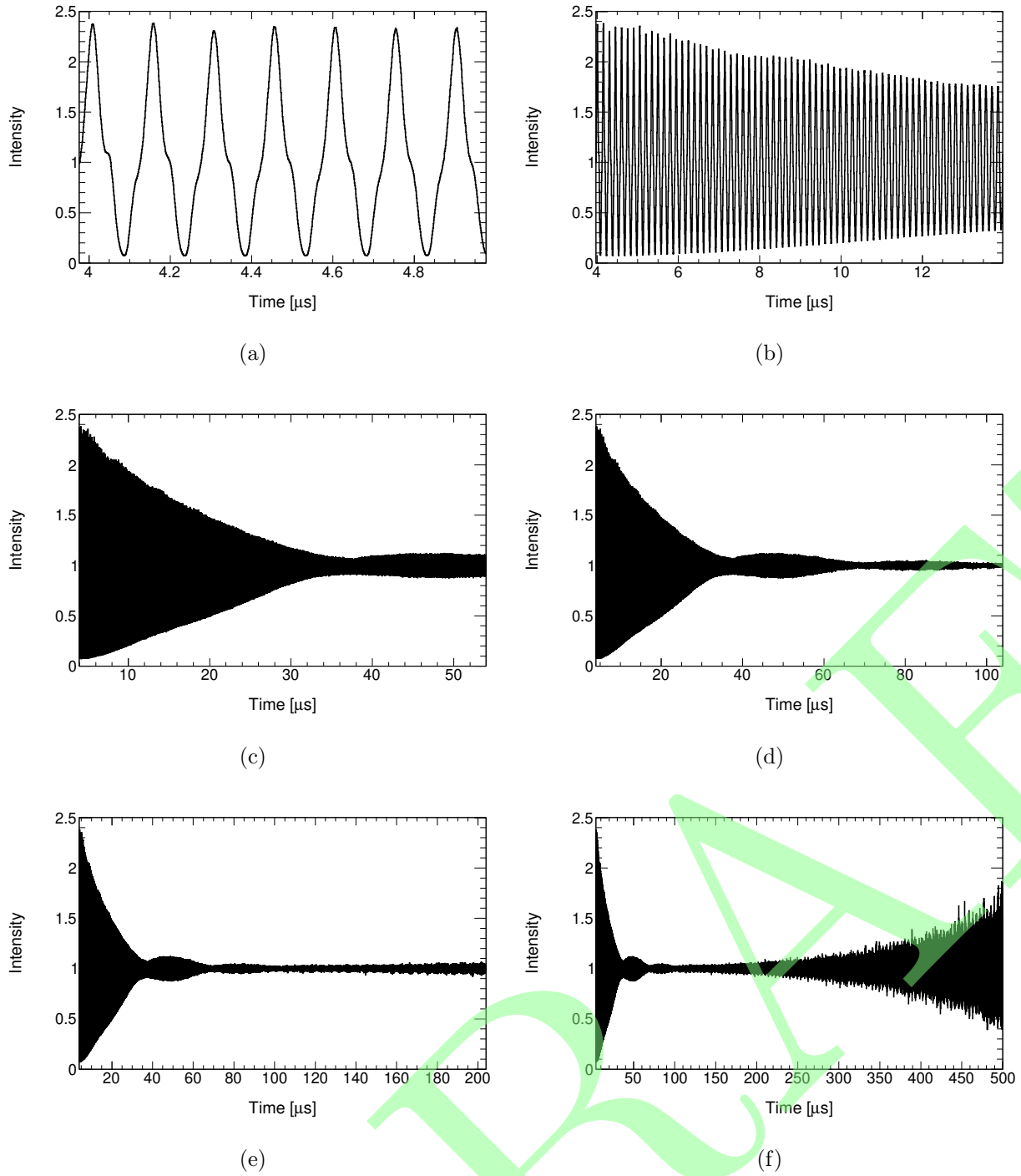


FIG. 4. Fast rotation signal as a function of time as seen by all the calorimeters combined for the Run-1 9-day data set for the time ranges: (a) 4-5, (b) 4-14, (d) 4-54, (e) 4-104, (f) 4-204 and (g) 4-504 μs with respect to the beam injection. The time interval is 1 ns. The modulation with a 35 μs period corresponds to the beam partially and slowly re-bunching due to its asymmetric momentum distribution. This could potentially also be a sign of time-momentum correlation in the incoming beam profile.

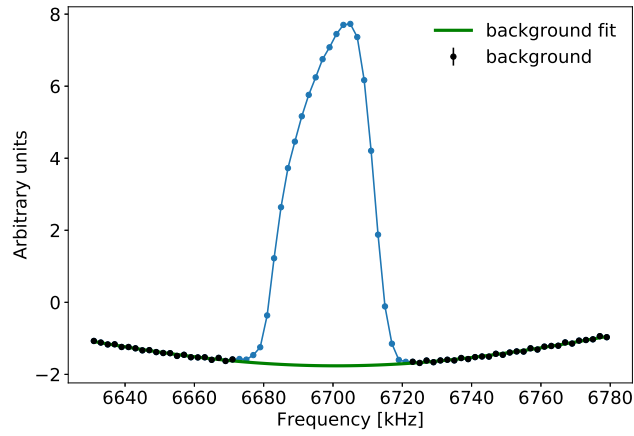
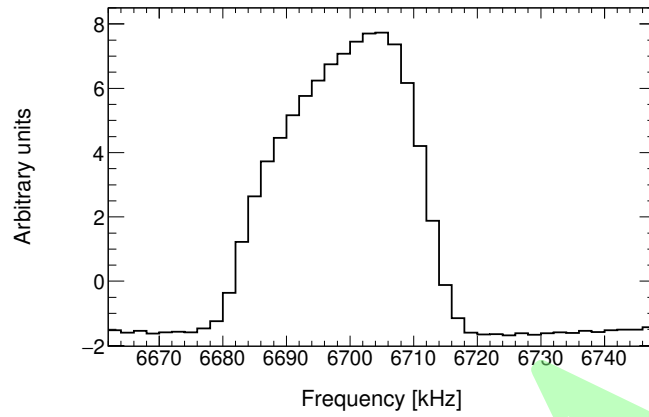
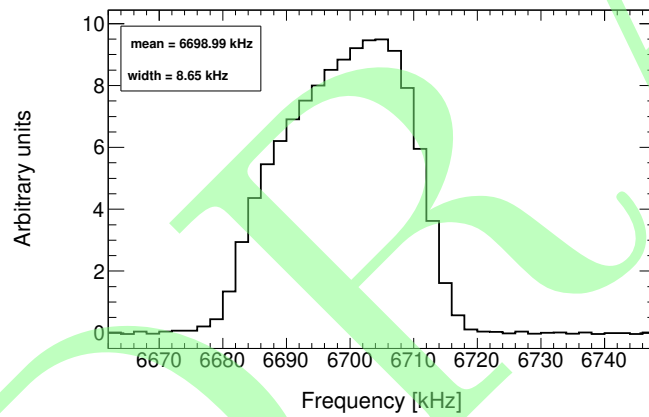


FIG. 5. Optimum cardinal sine background fit to the cosine Frequency distribution.

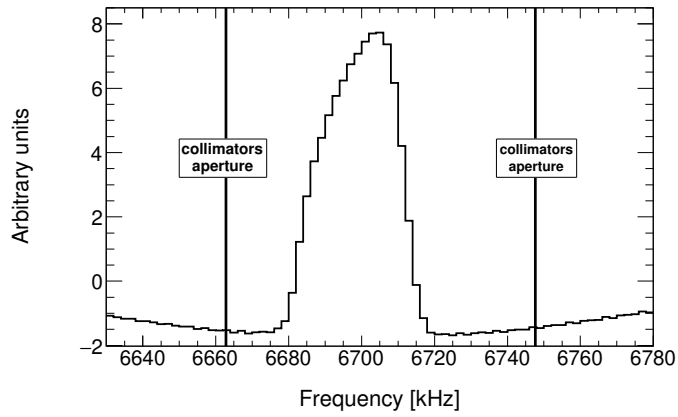


(a)

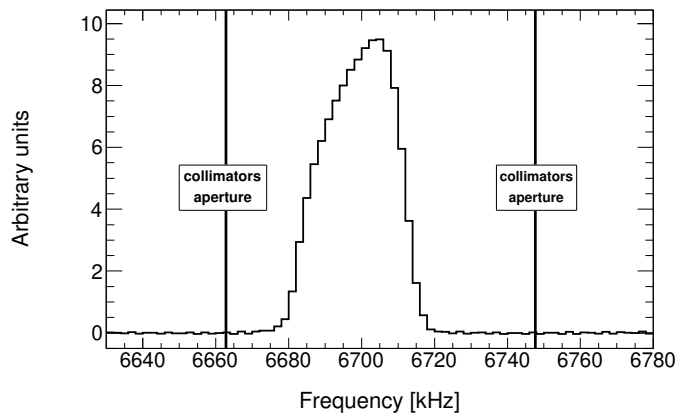


(b)

FIG. 6. Frequency distributions: (a) cosine Fourier transform, and (b) corrected cosine Fourier transform limited to the collimator aperture.



(a)



(b)

FIG. 7. Frequency distributions: (a) cosine Fourier transform, and (b) corrected cosine Fourier transform for the full frequency range used in the analysis.

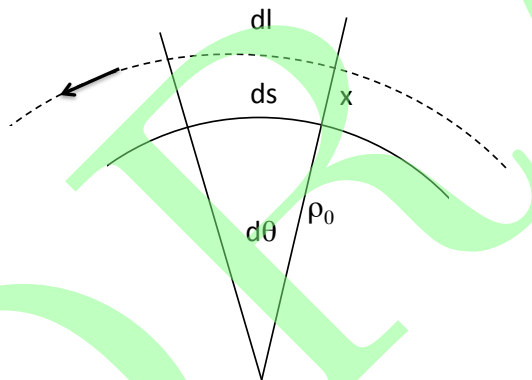


FIG. 8. Curvilinear coordinate system. The integrated path length for the part of the trajectory at $\rho > \rho_0$ is greater than the length of the path for $\rho < \rho_0$.

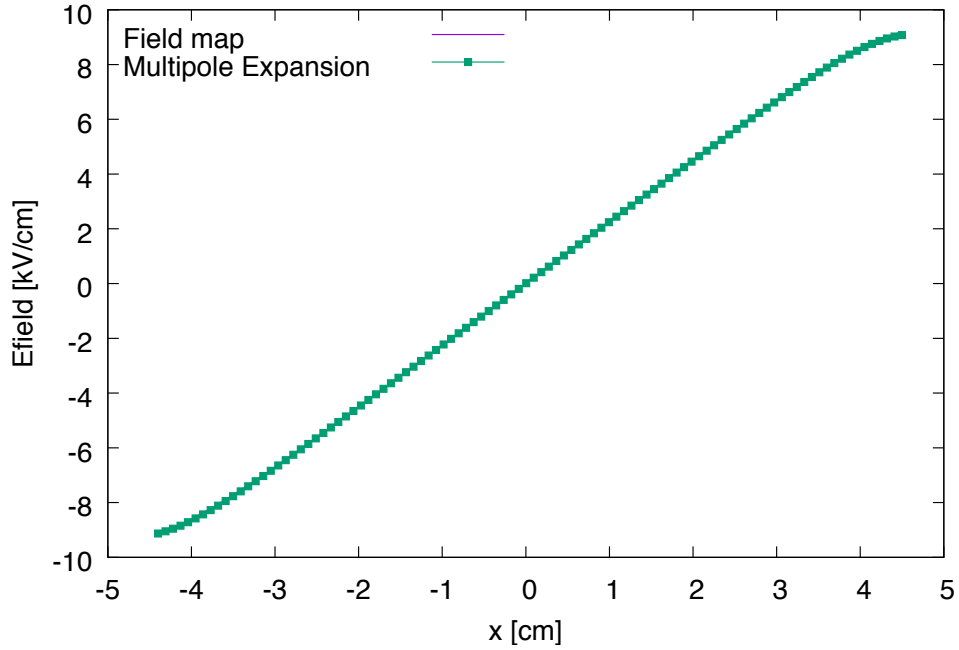


FIG. 9. Electric field along the x-axis in the midplane ($y=0$). The green points are computed from the multipole expansion using Equation 15 and the coefficients in Table ???. The 'purple' curve (hidden by the green points) are the values from the field map.

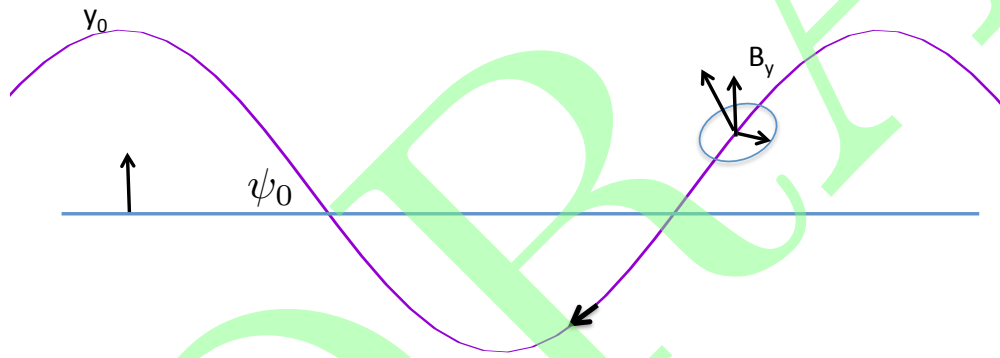


FIG. 10. pitching trajectory

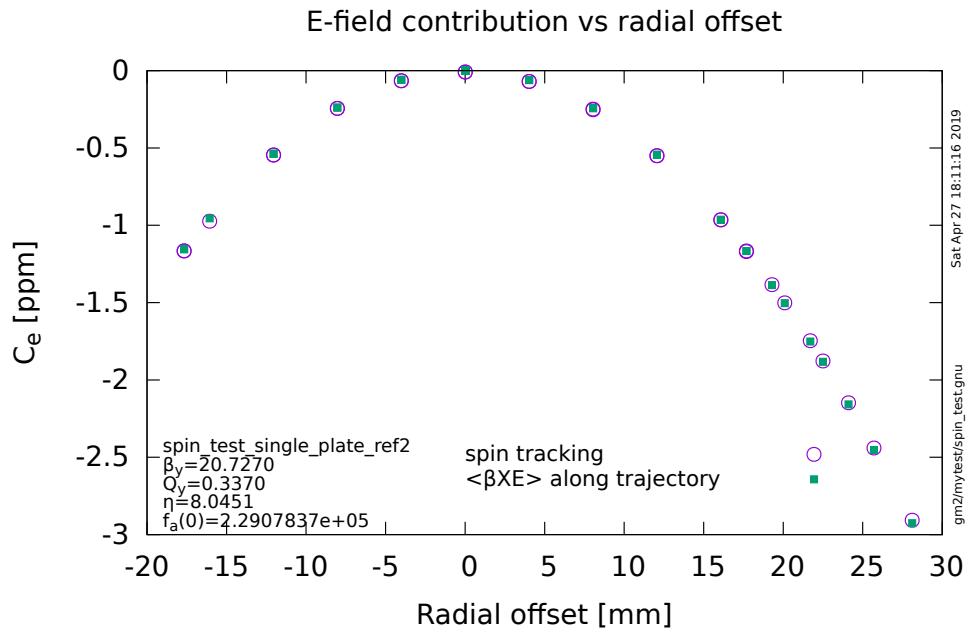


FIG. 11. Spin tracking and integration

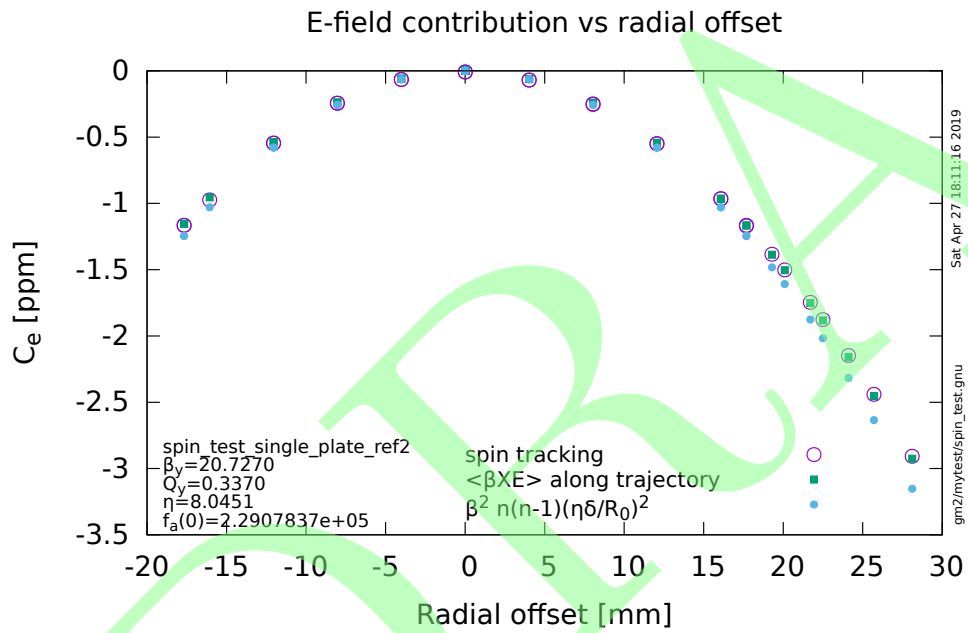


FIG. 12. Spin tracking, integration, linear

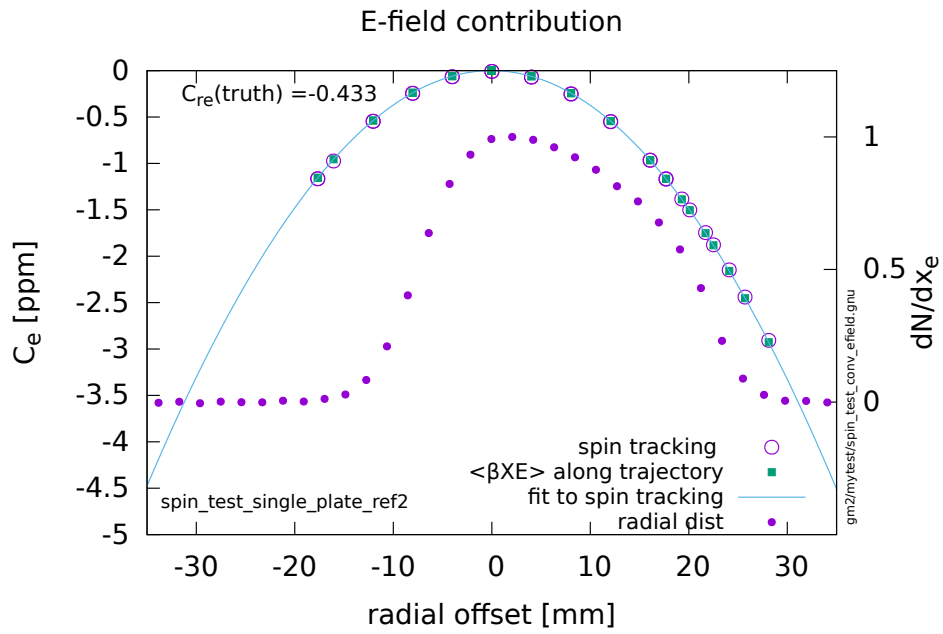


FIG. 13. Spin tracking and integration and convolve

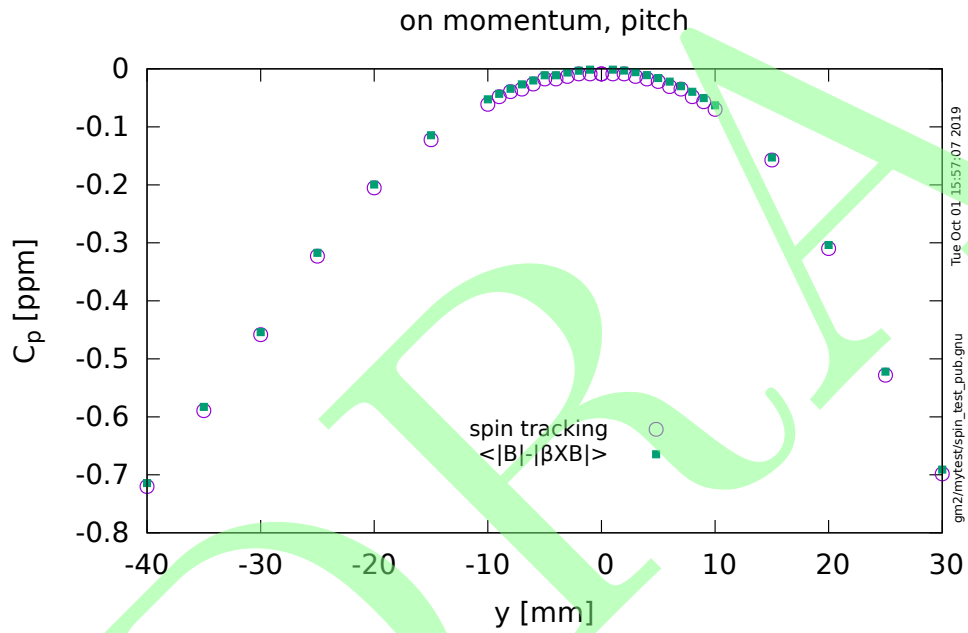


FIG. 14. Spin tracking and integration

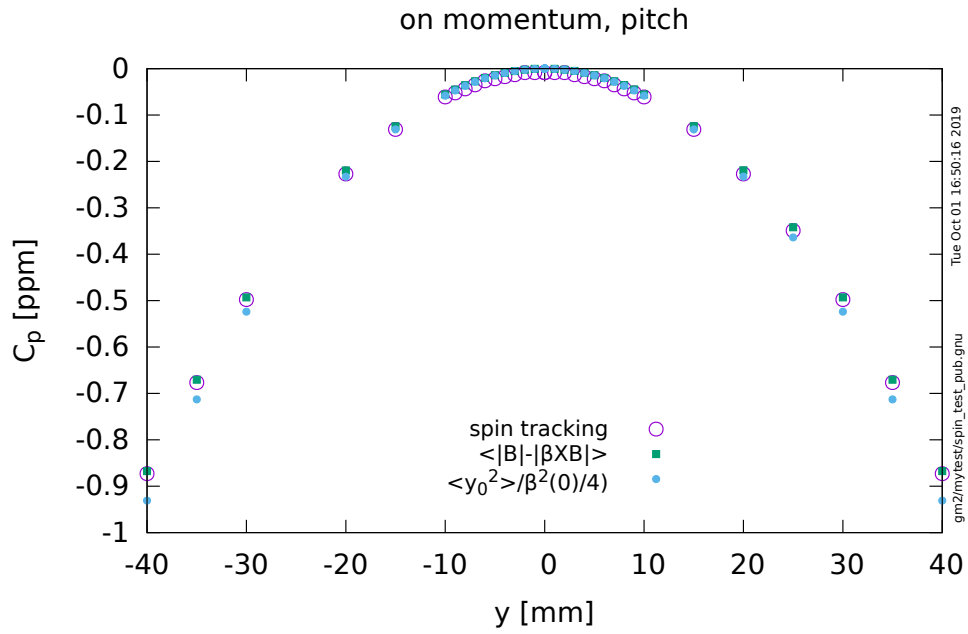


FIG. 15. Spin tracking, integration, linear

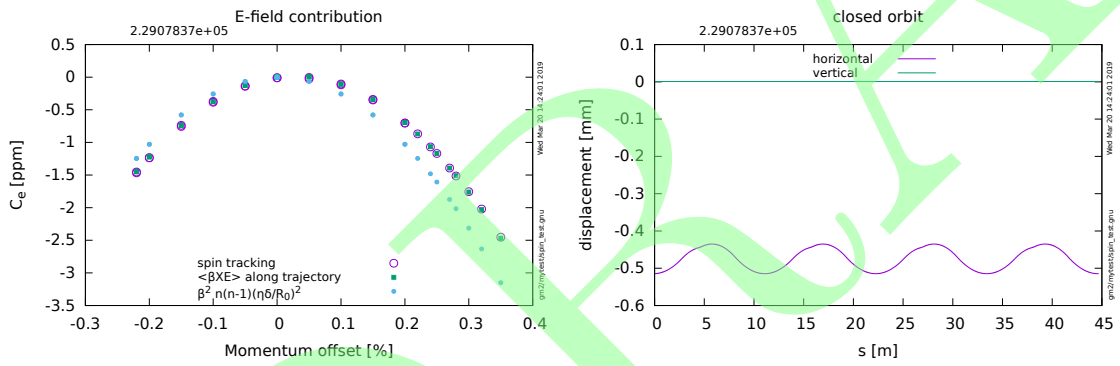


FIG. 16. E-field alignment error

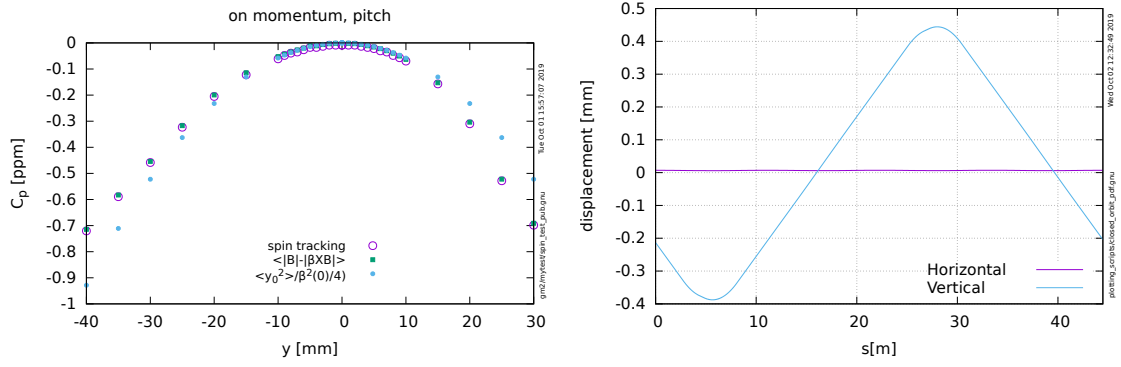


FIG. 17. pitch alignment error

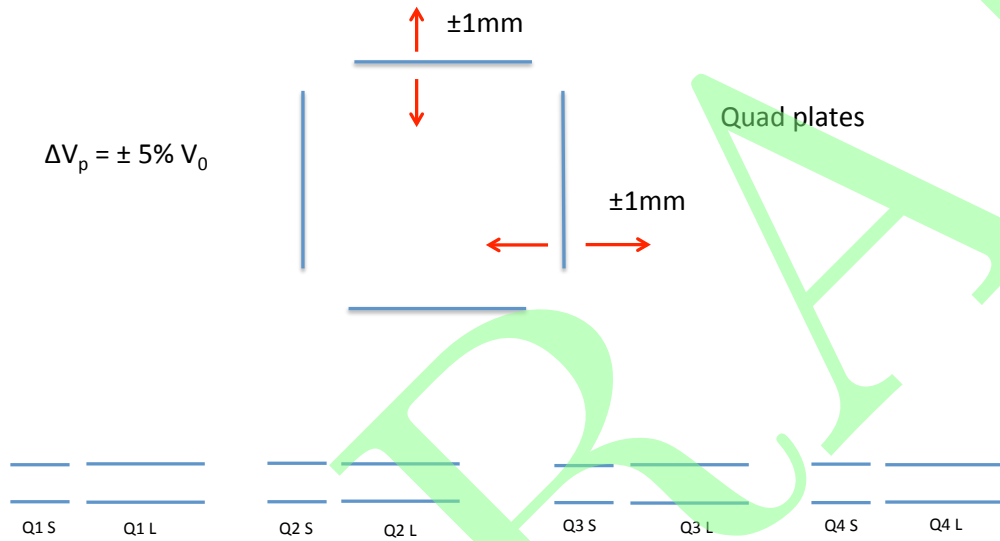


FIG. 18. Quad plate voltage and alignment errors

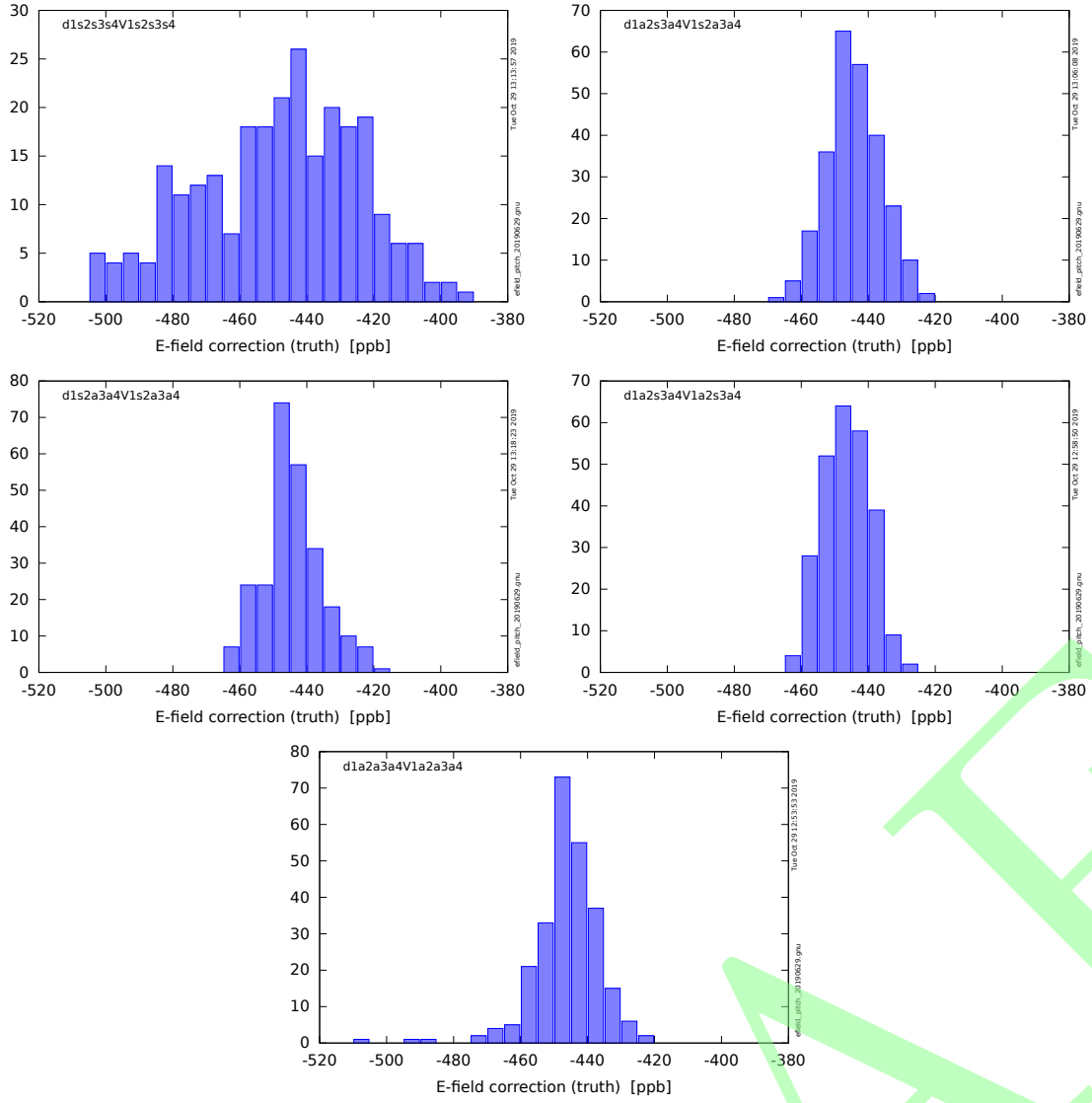


FIG. 19. Distribution of contribution of electric field to ω_a for four distinct sets of permutations

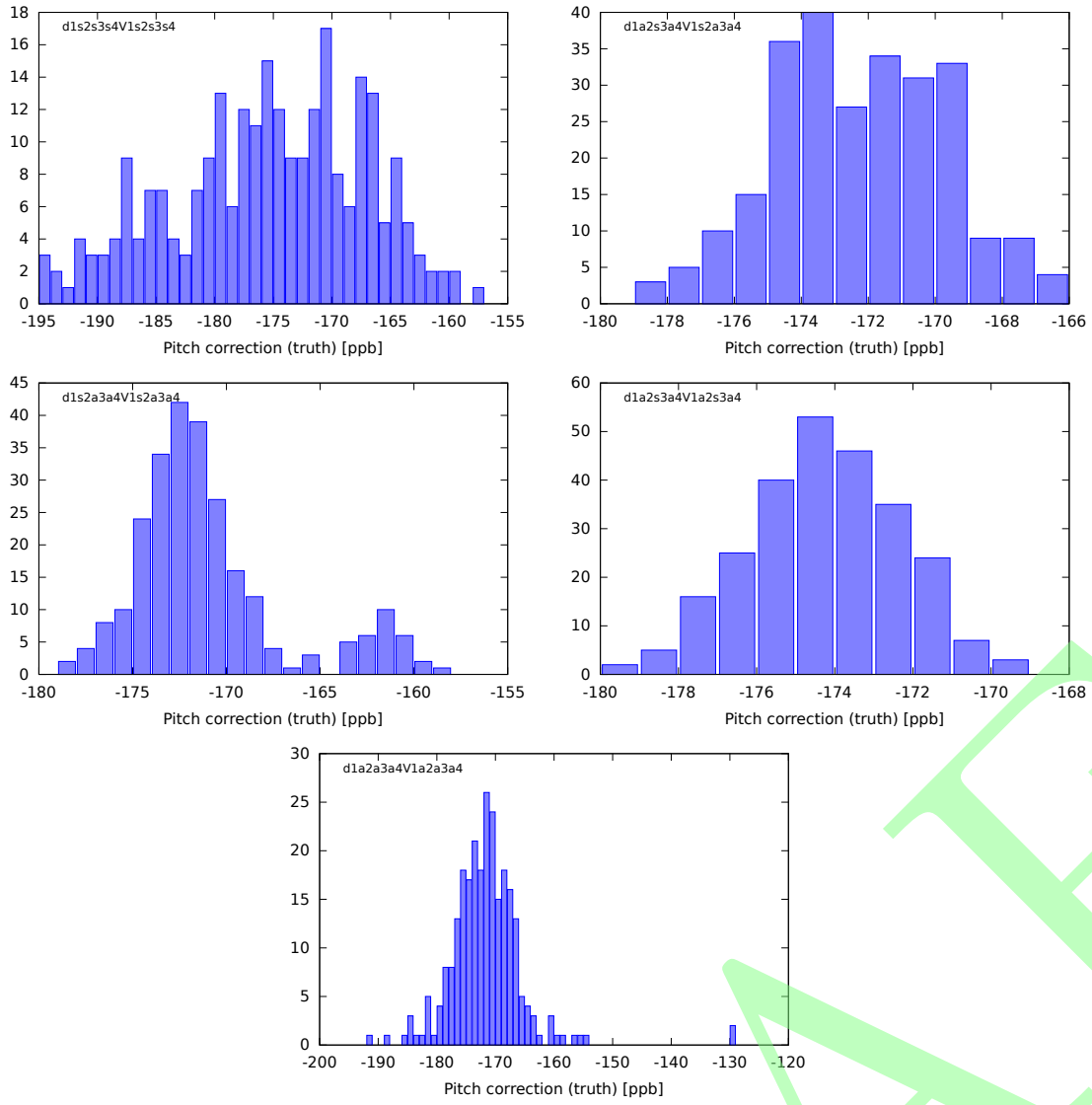


FIG. 20. Distribution of contribution from pitch to ω_a for four distinct sets of permutations.

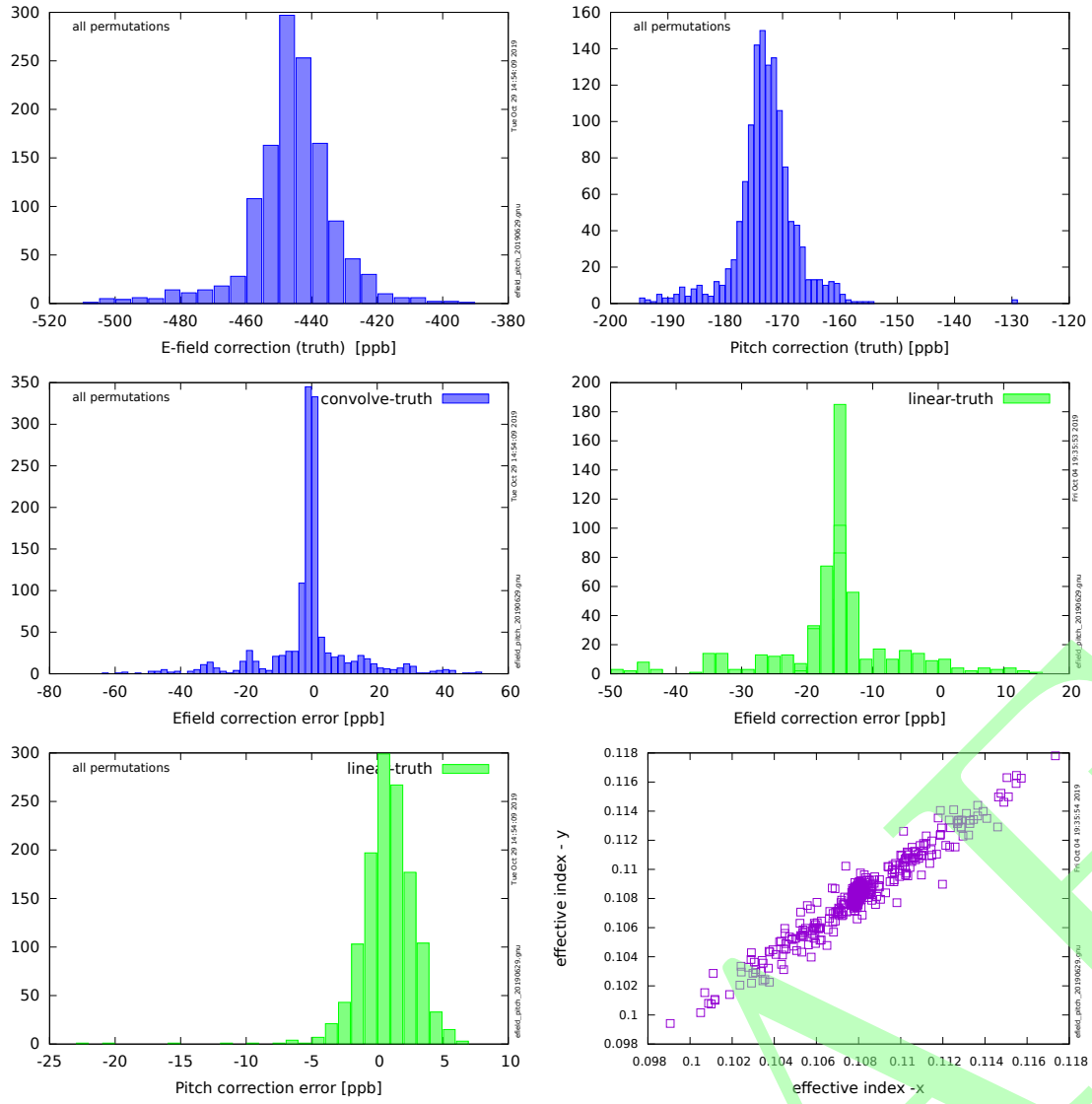


FIG. 21. Distribution of contribution from pitch to ω_a for all permutations.